Amino Acids (2012) 42:1329–1337
DOI 10.1007/s00726-010-0827-5

ORIGINAL ARTICLE

A Cy5.5-labeled phage-displayed peptide probe for near-infrared fluorescence imaging of tumor vasculature in living mice

Kai Chen · Li-Peng Yap · Ryan Park · Xiaoli Hui · Kaichun Wu · Daiming Fan · Xiaoyuan Chen · Peter S. Conti

Received: 26 October 2010 / Accepted: 20 December 2010 / Published online: 7 January 2011

Abstract Near-infrared (NIR) fluorescence optical imaging is an emerging imaging technique for studying diseases at the molecular level. Optical imaging with a NIR emitting fluorophore for targeting tumor vasculature offers a noninvasive method for early detection of tumor angiogenesis and efficient monitoring of response to anti-tumor vasculature therapy. The previous in vitro results demonstrated that the GX1 peptide, identified by phage-display technology, is a tumor vasculature endothelium-specific ligand. In this report, Cy5.5-conjugated GX1 peptide was evaluated in a subcutaneous U87MG glioblastoma xenograft model to investigate tumor-targeting efficacy. The in vitro flow cytometry results revealed dose-dependent binding of Cy5.5-GX1 peptide to U87MG glioma cells. In vivo optical imaging with the Cy5.5-GX1 probe exhibited rapid U87MG tumor targeting at 0.5 h p.i., and high tumor-to-background contrast at 4 h p.i. Tumor specificity of Cy5.5-GX1 was confirmed by effective blocking of tumor uptake in the presence of unlabeled GX1 peptide (20 mg/kg). Ex vivo imaging further confirmed in vivo imaging findings, and demonstrated that Cy5.5-GX1 has a tumor-to-muscle ratio (15.21 ± 0.84) at 24 h p.i. for the non-blocked group and significantly decreased ratio (6.95 ± 0.75) for the blocked group. In conclusion, our studies suggest that Cy5.5-GX1 is a promising molecular probe for optical imaging of tumor vasculature.

Keywords Molecular imaging probe · Phage-displayed peptide · Fluorescence imaging · Tumor vasculature

Abbreviations

NIRF	Near-infrared fluorescence
HPLC	High performance liquid chromatography
p.i.	Postinjection
GX1	Cyclo(CGNSNPKSC) peptide
PBS	Phosphate buffered saline
Boc	*t*-Butoxycarbonyl
NHS	*N*-hydroxysuccinimide
TFA	Trifluoroacetic acid
TIS	Triisopropylsilane
DMSO	Dimethyl sulfoxide
DIPEA	Diisopropylethylamine

K. Chen (✉) · L.-P. Yap · R. Park · P. S. Conti (✉)
Molecular Imaging Center, Department of Radiology, Keck School of Medicine, University of Southern California, 2250 Alcazar Street, CSC 103, Los Angeles, CA 90033-9061, USA
e-mail: chenkai@usc.edu

P. S. Conti
e-mail: pconti@usc.edu

X. Chen
Laboratory of Molecular Imaging and Nanomedicine (LOMIN), National Institute of Biomedical Imaging and Bioengineering (NIBIB), National Institutes of Health (NIH), Bethesda, MD 20892, USA

X. Hui · K. Wu · D. Fan
State Key Laboratory of Cancer Biology and Institute of Digestive Diseases, Xijing Hospital, The Fourth Military Medical University, Xi'an 710032, Shanxi, China

Introduction

Near-infrared fluorescence (NIRF) optical imaging offers a noninvasive method for studying diseases at the molecular level in living subjects (Weissleder and Mahmood 2001; Tung 2004; Kobayashi et al. 2010). As an excellent

complement to nuclear imaging techniques, optical imaging uses neither ionizing radiation nor radioactive materials and is relatively inexpensive, robust, sensitive, and straightforward (Chen et al. 2004). The major limitations of optical imaging are absorption and scattering that occur in biological tissues which limit penetration of light through the body. However, biological tissues have reduced absorbance and autofluoresence in the NIR region (650–900 nm), which allows efficient photon penetration into and out of tissue with lower intra-tissue scattering. In addition, the shorter path-length of light makes optical imaging more feasible in small animals (Cheng et al. 2005). Recent advances in molecular imaging have demonstrated that optical imaging, NIRF in particular, can be used to monitor the biological activity of a wide variety of molecular targets, including cell surface receptors (Ke et al. 2003; Achilefu et al. 2000, 2002; Chen et al. 2004; Cheng et al. 2005), intracellular enzymes (Weissleder et al. 1999; Tung et al. 2004; Mahmood and Weissleder 2003), and antigens (Moore et al. 2004), providing a unique opportunity to quantitatively evaluate the biological events associated with various diseases. As such, NIRF optical imaging can make significant impacts in better understanding of biology, early detection of disease, monitoring therapy response, and guiding drug discovery and development.

Angiogenesis, the formation of new blood vessels from pre-existing vasculature, is a fundamental process occurring during tumor progression (Cai et al. 2008; Chen and Chen 2011). Current evidence suggests tumor-vasculature formation is a complex multi-step process that follows a characteristic sequence of events mediated and controlled by growth factors, cellular receptors and adhesion molecules (Ellis et al. 2001; Kuwano et al. 2001; Yancopoulos et al. 2000). Differences between tumor angiogenesis and physiological angiogenesis exist and include aberrant vascular structure, altered endothelial cell-pericyte interactions, abnormal blood flow, increased permeability, and delayed maturation (Bergers and Benjamin 2003; Hanahan and Folkman 1996). Because tumor vasculature plays a vital role in tumor growth and metastasis (Cai et al. 2008; Weissleder 2006), it is of great importance to develop molecular probes for imaging tumor vasculature in living subjects. In vivo angiogenesis specific molecular probes will aid in metastasis detection, tumor biology of angiogenesis, and facilitate the development of anti-tumor vasculature therapy.

To date, target-specific delivery of molecular imaging probes has employed numerous targeting moieties, including small molecules, peptides, proteins, antibodies, antibody fragments, and nanoparticles (Chen and Chen 2010). Among these targeting moieties, low-molecular-weight small peptides demonstrate a number of distinct advantages over others. In particular, small peptides have favorable pharmacokinetic and tissue distribution patterns, increased permeability, lower toxicity, lower immunogenicity, and considerable flexibility in chemical modification (Chen and Chen 2010). Development of peptide-based molecular imaging probes has customarily relied on (1) isolation of naturally occurring peptides, (2) screening synthetic peptide libraries, and (3) structure-based rational design. An alternative technique involves the screening of bacteriophage (phage) display libraries. Since its inception almost 30 years ago, phage display has become a powerful technique that allows vast sequence space screening, providing a means to improve peptide affinity and generate unique peptides that bind any given target (Deutscher 2010).

Through in vivo screening of a phage-display peptide library, we previously identified a cyclic 9-mer peptide, CGNSNPKSC, named GX1, which binds specifically to the human gastric cancer vasculature (Chen et al. 2009; Zhi et al. 2004; Hui et al. 2008). Immunohistochemical staining, enzyme-linked immunosorbent assay (ELISA), and immunofluorescence confirmed the targeting activity of GX1 peptide, indicating that GX1 might be used as a novel vascular marker for human cancers (Hui et al. 2008; Zhi et al. 2004). In this report, we conjugated GX1 peptide with NIR fluorescent dye Cy5.5. The resulting Cy5.5-GX1 probe was evaluated for NIR imaging of tumor vasculature using the U87MG tumor xenograft mouse model.

Materials and methods

General

All chemicals (reagent grade) were obtained from commercial suppliers and used without further purification. The Boc-protected GX1 peptide was purchased from C S Bio, Inc. (Menlo Park, CA, USA). Cy5.5 monofunctional NHS ester (Cy5.5-NHS) was purchased from GE Healthcare (Piscataway, NJ, USA). Analytical and semi-preparative reversed phase HPLC was accomplished on two Waters 515 HPLC pumps, a Waters 2487 absorbance UV detector, which were operated by Waters Empower 2 software. The UV absorbance was monitored at 214 and 254 nm. Mass spectra were obtained on a Q-Tof premier-UPLC system equipped with an electrospray interface (ESI) (Waters, USA).

Synthesis of Cy5.5-GX1 peptide

Boc-protected GX1 peptide (0.5 mg, 0.497 μmol, 1 equiv.) was dissolved in 100 μL of DMSO and mixed with Cy5.5-NHS (0.56 mg, 0.497 μmol. 1 equiv.) in DIPEA (10 μL) in the dark. Sonication was performed in the dark at 45°C for 2 h. The reaction was then quenched with 50 μL of 5% acetic acid (HOAc). Purification of the crude product was

performed on a reversed phase HPLC system using a semi-preparative Phenomenex Luna C_{18} column (250 × 10 mm). The flow rate was 3 mL/min, with the gradient mobile phase starting from 95% solvent A (0.1% TFA in water) and 5% solvent B (0.1% TFA in acetonitrile; 0–2 min) to 35% solvent A and 65% solvent B at 30 min. The peak containing the Boc-protected Cy5.5-GX1 peptide was collected and lyophilized with a 66% yield (0.62 mg). The Boc-protected Cy5.5-GX1 peptide (0.5 mg, 0.263 μmol, 1 equiv.) was dissolved in 250 μL of TFA:TIS:water (95:2.5:2.5) solution. The mixture was stirred at room temperature for 1 h and evaporated. The residue was redissolved in 0.5 mL of water and the crude product was purified on a Phenomenex Luna C_{18} reversed phase column (5 μm, 250 × 10 mm). The flow rate was 3 mL/min for semi-preparative HPLC, with the gradient mobile phase starting from 100% solvent A (0.1% TFA in water) to 60% solvent A and 40% solvent B at 30 min. Analytical HPLC was performed on a Phenomenex Luna C_{18} reversed phase analytic column (5 μm, 250 × 4.6 mm). The flow rate was 1 mL/min with the gradient mobile phase starting from 100% solvent A (0.1% TFA in water) to 60% solvent A and 40% solvent B at 30 min. The Cy5.5-GX1 peptide was collected, lyophilized, and stored in the dark at −20°C until use (0.36 mg, yield: 76%).

Cell line and culture condition

U87MG human glioblastoma cell line was obtained from the American Type Culture Collection (ATCC, Manassas, VA, USA). U87MG glioma cells were grown in Dulbecco's modified medium (USC Cell Culture Core, Los Angeles, CA, USA) supplemented with 10% fetal bovine serum (FBS) at 37°C in humidified atmosphere containing 5% CO_2.

Flow cytometry analysis of cell binding

Human U87MG glioblastoma cells were used to determine cell binding of Cy5.5-GX1 peptide. To minimize the non-specific uptake of peptides by pinocytosis, incubations were performed on ice and followed immediately by flow cytometry. U87MG cells (1.5×10^6) were incubated with Cy5.5-GX1 peptide (0.5, 1 and 4 μg) for 60 min. The control group was cells incubated without Cy5.5-GX1. After washing with ice cold PBS (1 mL) three times, Cy5.5 fluorescence was determined using the BD™ LSR II flow cytometer (a special order research product, BD Biosciences, San Jose, CA, USA). The fluorescence profiles and binding percentages of the cell populations were obtained and analyzed using FACSDiva v 6.0 (BD Biosciences, San Jose, CA, USA).

Animal model

All animal studies were performed according to a protocol approved by the University of Southern California Institutional Animal Care and Use Committee. Female athymic nude mice (about 4–6 weeks-old, with a body weight of 20–25 g) were obtained from Harlan (Livermore, CA, USA). The U87MG human glioma xenograft model was generated by subcutaneous injection of 5×10^6 U87MG human glioma cells suspended in 100 μL of PBS into the right shoulder of mice. The cells were allowed to grow 3–5 weeks until tumors were 200–500 mm^3 in volume. Tumor growth was measured using caliper measurements in orthogonal dimensions.

In vivo and ex vivo near-infrared fluorescence imaging

In vivo fluorescence imaging was performed using the IVIS Imaging System 200 Series and analyzed using the IVIS Living Imaging 3.0 software (Caliper Life Sciences, Alameda, CA, USA). A Cy5.5 filter set was used for acquiring the fluorescence of Cy5.5-conjugated GX1 peptide. Identical illumination settings (lamp voltage, filters, f/stop, field of views, binning) were used for acquiring all images. Fluorescence emission images were normalized and reported as photons per second per centimeter squared per steradian (p/s/cm^2/sr). The non-blocked mice ($n = 3$) received 1.0 nmol of Cy5.5-GX1 peptide intravenously and subjected to optical imaging at various time points post-injection. The blocked group of mice ($n = 3$) were injected with a mixture of 20 mg/kg of unlabeled GX1 peptide and 1.0 nmol Cy5.5-GX1 peptide. All near-infrared fluorescence images were acquired using 1 s exposure time (f/stop = 4). Mice from non-blocked and blocked groups were euthanized at 24 h p.i. The tumors, tissues, and organs were dissected and subjected to ex vivo fluorescence imaging. The mean fluorescence for each sample was reported.

Data processing and statistical analysis

All of the data are given as means ± SD (standard deviation) of n independent measurements. Statistical analysis was performed with a Student's t test. Statistical significance was assigned for P values < 0.05. To determine tumor contrast, mean fluorescence intensities of the tumor (T) area at the right shoulder of the animal and of the normal tissue (N) at the surrounding tissue were calculated using the region-of-interest (ROI) function of the Living Image 3.0 software. Dividing T by N yielded the contrast between tumor and normal tissue.

Results

Synthesis and characterization of Boc-protected Cy5.5-GX1 peptide and Cy5.5-GX1 peptide

The schematic molecular structure of Cy5.5-GX1 conjugate is shown in Fig. 1. Preparation of Cy5.5-GX1 peptide was achieved in two steps with an overall yield of 50%. During the first step, the Cy5.5 fluorophore was conjugated to the N-terminal amino group of the cysteine residue while the amino group of the lysine side chain remained protected with *tert*-butyloxycarbonyl (Boc) group. After Boc deprotection in TFA, the Cy5.5-GX1 peptide probe was isolated through HPLC purification. The purity of the final product was over 97%. The retention time of Cy5.5-GX1 on analytical HPLC was 20.0 min. ESI high-resolution mass spectrometry yielded $m/z = 951.6077$ ($[M_r/2 - 1]^-$) for Boc-protected Cy5.5-GX1 (calculated $M_r = 1{,}904.5349$ for $C_{79}H_{106}N_{15}O_{28}S_6$) and $m/z = 901.5577$ ($[M_r/2 - 1]^-$) for Cy5.5-GX1 (calculated $M_r = 1{,}804.5138$ for $C_{74}H_{98}N_{15}O_{26}S_6$).

Flow cytometric analysis

The binding specificity of Cy5.5-GX1 to tumor cells was determined by flow cytometry studies. U87MG glioma cells (1.5×10^6) were incubated with 0–4 μg of Cy5.5-GX1 peptide for 60 min and measured using flow cytometry. The representative examples of flow cytometric analysis with various amount of Cy5.5-GX1 are plotted in Fig. 2a. The percentages of cells binding increased as a function of Cy5.5-GX1 concentration as shown in the histogram plot in Fig. 2b.

In vivo fluorescence imaging with Cy5.5-GX1

NIR fluorescence images of U87MG xenograft nude mice were acquired after intravenous injection of 1.0 nmol of Cy5.5-GX1 (Fig. 3a). Cy5.5-GX1 uptake in the U87MG tumor was imaged and showed the high contrast to background tissue during 0.5–24 h p.i. The Cy5.5-GX1 probe exhibited a rapid U87MG tumor targeting as early as 0.5 h p.i., and excellent tumor-to-background contrast at 4 h p.i. Fluorescence intensities in the tumor and the normal tissues were plotted as a function of time (Fig. 3b). The tumor tissue uptake reached a maximum at 1 h p.i. and slowly washed out over time. In contrast, normal tissue had faster probe binding and washout. The overall uptake of Cy5.5-GX1 in normal tissue was much lower compared to tumor during the 24 h period studied.

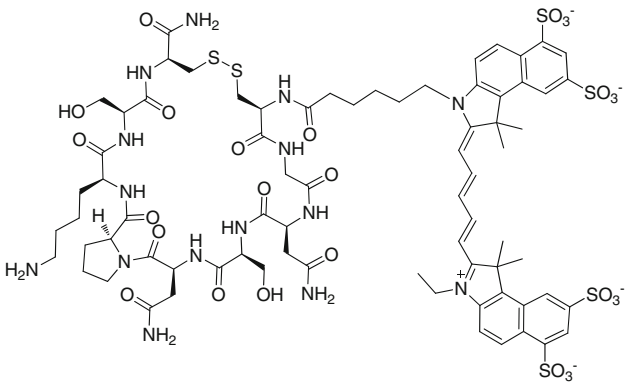

Fig. 1 Schematic structure of the Cy5.5-GX1 conjugate

To validate the targeting specificity of the Cy5.5-GX1 probe, a blocking experiment was performed. For the blocked group, each U87MG-tumor-bearing mouse was intravenously co-injected with 1.0 nmol of Cy5.5-GX1 and 20 mg/kg unlabeled GX1 peptide, whereas mice in the non-blocked group were injected with 1.0 nmol of Cy5.5-GX1 only. In Fig. 4a, NIR fluorescence imaging of U87MG-tumor-bearing mice at 4 h p.i. from the non-blocked group and blocked group are presented on the left and right, respectively. At 4 h, the non-specific binding was probably cleared out from the animals. Unlabeled GX1 peptide significantly reduced tumor uptake in blocked scans compared with the non-blocked group.

Furthermore, ex vivo evaluation of excised organs showed Cy5.5-GX1 was predominantly taken up by the U87MG tumor at 24 h p.i. (Fig. 4b), as seen in the in vivo imaging results. Fluorescence intensities of tumor and organs were quantified using regions of interest (ROIs) that encompassed the entire organ. Data from quantitative analysis are plotted in Fig. 4c. In the non-blocked group, Cy5.5-GX1 showed excellent tumor uptake with minimal amounts in other major organs. Co-injections of Cy5.5-GX1 with unlabeled GX1 peptide reduced the overall probe uptake and Cy5.5-GX1 was not noticeable in the tumor, suggesting the targeted specificity of the Cy5.5-GX1 probe. Based on quantitative analysis of ex vivo imaging, the contrast ratios of tumor to normal organs for non-blocked and blocked groups were calculated and presented in Fig. 4d. Comparison data between the groups demonstrated that Cy5.5-GX1 has a tumor-to-muscle ratio (15.21 ± 0.84) at 24 h p.i. in the non-blocked group and significantly decreased ratio (6.95 ± 0.75) in the blocked group. In addition, the non-blocked group ratio of tumor-to-liver and tumor-to-kidney uptake at 24 h p.i. was calculated to be 4.02 ± 0.13 and 7.98 ± 0.44, respectively, while the corresponding values for the blocked group were 2.79 ± 0.35 and 4.67 ± 0.55, respectively.

Discussion

Molecular imaging has emerged because of unprecedented advances in molecular and cell biology, discovery of

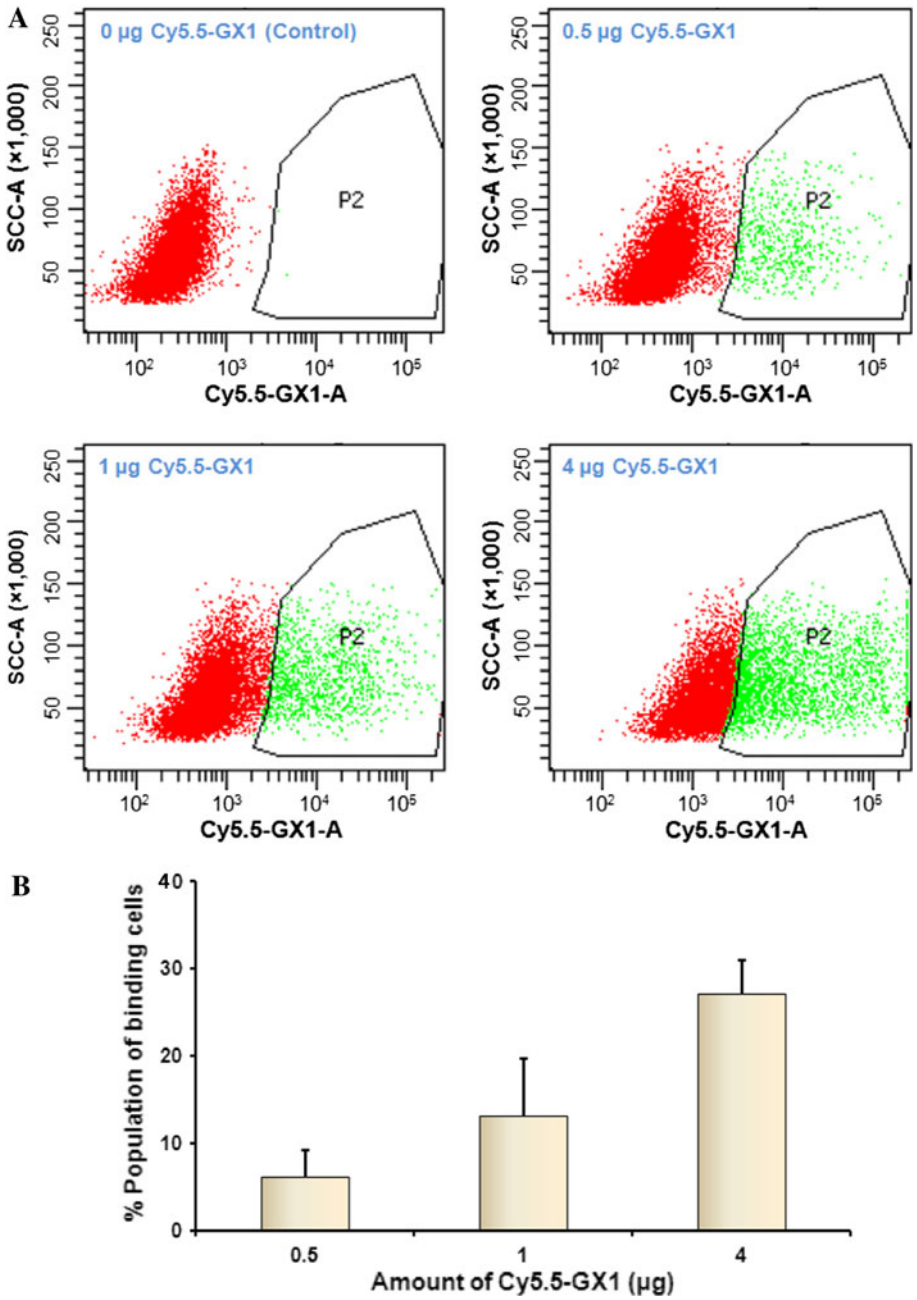

Fig. 2 In vitro binding of Cy5.5-GX1 to U87MG glioma cells as determined by flow cytometry. **a** Plots are representative examples of flow cytometry analysis after 1 h incubation with various amounts of Cy5.5-GX1. The control group was cells incubated without Cy5.5-GX1. **b** Histogram plot of flow cytometry results showing dose-dependent binding pattern of Cy5.5-GX1 to U87MG glioma cells

numerous molecular probes, and successful development of small-animal imaging instrumentation (Chen et al. 2004). This emergence has created the opportunity to bridge established in vitro findings with potential disease interventions in the clinical setting (Chen et al. 2004). Just as the predominant imaging modalities in nuclear medicine, positron emission tomography (PET) and single photon emission computed tomography (SPECT) gained their power in patient management through the use of radiolabeled probes (Chen and Conti 2010; Chen and Chen 2011), the underlying principles can also be tailored to other molecular imaging modalities such as optical imaging. With the pivotal role offered through new imaging probes, the design and development of biologically active probes has become one of the major research areas of molecular imaging (Massoud and Gambhir 2003; Gambhir 2002; Weissleder 2006).

One such development is to image angiogenesis, one of the key requirements during cancer progression. Without angiogenesis, the tumor may not grow beyond a few millimeters in diameter (Bergers and Benjamin 2003; Folkman 1995). Through the leaky tumor vasculature, cancer cells can break away or spill from a primary tumor, circulate through the bloodstream, and undergo expansive growth to

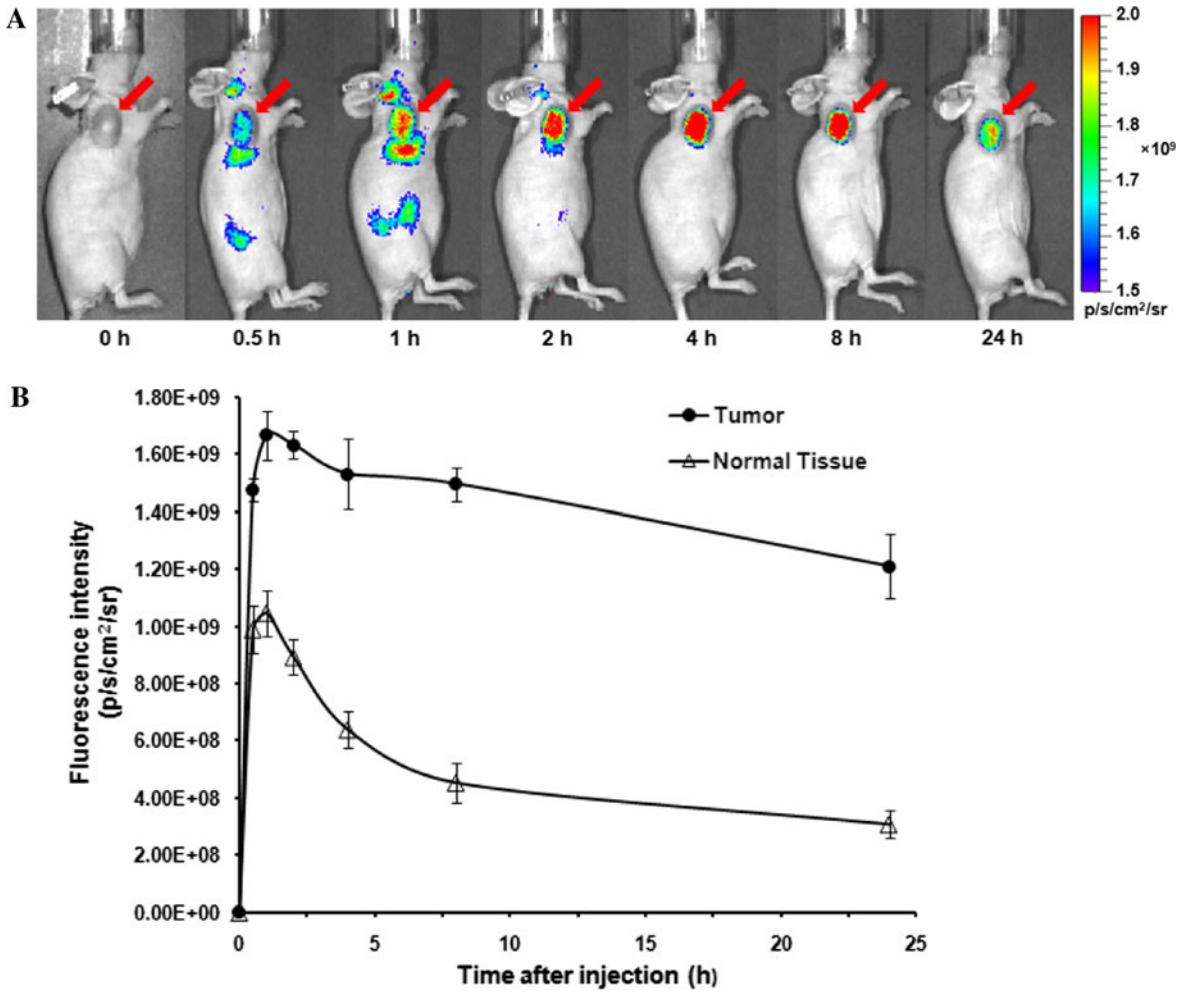

Fig. 3 **a** In vivo fluorescence imaging of subcutaneous U87MG tumor-bearing nude mice after intravenous injection of 1.0 nmol of Cy5.5-GX1. The tumor can be clearly visualized as indicated by *arrows* from 0.5 to 24 h p.i. The fluorescence intensity was recorded as per second per centimeter squared per steradian (p/s/cm^2/sr). **b** Quantification and kinetics of in vivo targeting character of Cy5.5-GX1. Tumor fluorescence washout was slower than that in normal tissue

metastasize within the parenchyma of other organ(s). The fact that tumor progression is dependent on angiogenesis has inspired scientists to search for anti-angiogenic molecules and design anti-angiogenic strategies for cancer treatment and prevention of cancer recurrence/metastasis (Cai and Chen 2006; Folkman 2007; Kerbel and Folkman 2002). During the last two decades, the research field of angiogenesis has rapidly expanded and provided an increasing body of evidence that inhibition of angiogenesis could attenuate tumor growth. A large series of inhibitors of angiogenesis have shown great potential in the treatment of cancer in preclinical research and clinical studies. To evaluate the effects of these new anti-angiogenic agents, it would be of great interest to image the process of angiogenesis in tumors. To date, several markers have been identified that express on newly formed blood vessels in tumors and in the extracellular matrix surrounding newly formed blood vessels (Charnley et al. 2009; Ocak et al. 2007; Beer and Chen 2010).

Using angiogenesis as a target, phage-display technology was used to identify our molecular probe. Phage display technology is a powerful approach for the generation of peptides that target specific organ- or tumor-structures (Ueberberg and Schneider 2010). Since its inception almost 30 years ago, phage display has been utilized in vitro, in situ, and in vivo to isolate peptides that bind numerous targets (Deutscher 2010). The GX1 peptide (sequence of CGNSNPKSC) was previously identified through in vivo screening using a phage-display peptide library and results showed the GX1 peptide bound specifically to the human gastric cancer vasculature (Chen et al. 2009; Zhi et al. 2004; Hui et al. 2008). The immunohistochemical staining, ELISA, and immunofluorescence studies indicate that GX1 might be used as a novel vascular marker for human

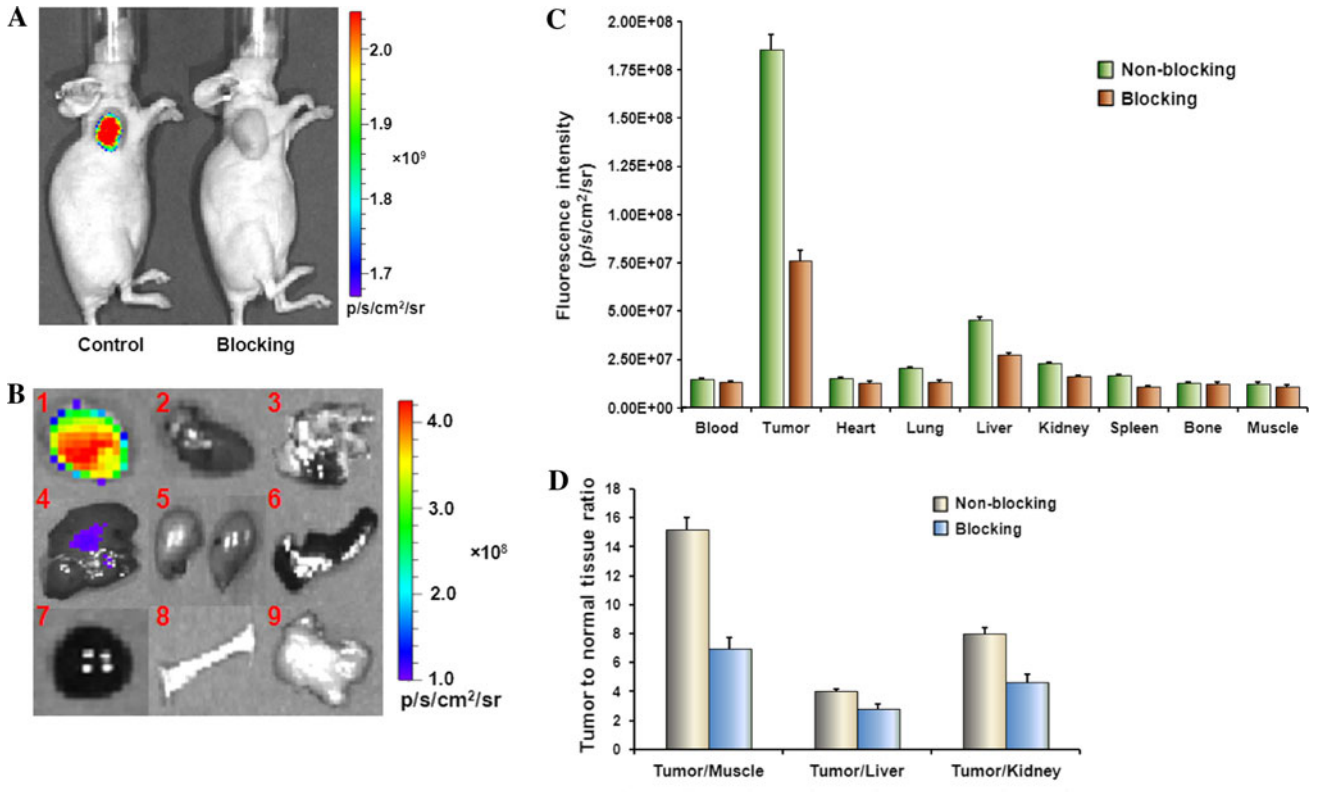

Fig. 4 **a** Representative optical imaging (acquired at 4 h p.i.) of mice bearing subcutaneous U87MG tumor on the right shoulder demonstrating blocking of Cy5.5-GX1 (1.0 nmol) uptake by co-injection with GX1 peptide (20 mg/kg). **b** Ex vivo imaging of tumor and normal tissues of Cy5.5-GX1 after euthanizing the mice at 24 h p.i.; *1* Tumor, *2* Heart, *3* Lung, *4* Liver, *5* Kidney, *6* Spleen, *7* Blood *8* Bone *9* Muscle. **c** ROI analysis of fluorescence intensity in ex vivo of major tissues with (Blocking) and without (Non-blocking) co-injection of GX1 peptide (20 mg/kg). **d** Fluorescence intensity ratio of tumor-to-normal tissue based on the ROI analysis. *Error bar* was calculated as the standard deviation ($n = 3$)

cancers (Hui et al. 2008; Zhi et al. 2004). Considering all of above factors, we hypothesized that fluorophore-conjugated GX1 peptide would generate a novel molecular probe for optical imaging of tumor vasculature.

To create the probe, we chose the Cy5.5 dye to conjugate with the GX1 peptide. The resulting Cy5.5-GX1 probe was subjected to in vitro testing. Flow cytometry analysis demonstrated Cy5.5-GX1 bound to U87MG glioma cells in a dose-dependent manner and suggest binding saturation did not occur from the 0.5–4 μg amounts of labeled peptide. In addition, the intracellular localization of Cy5.5-GX1 was also examined using confocal microscopy (data not shown). The results showed Cy5.5-GX1 was internalized into the U87MG cells rather than bound to the cell surface. This observation is in contrast to other peptide-based ligands that target to tumor vasculature receptors. For example, the internalization of integrin targeted probes, such as cyclic RGD peptide, does occur after binding to tumor cells yet in a very limited extent (Castel et al. 2001; Sancey et al. 2009). One possible explanation is the fluorescence dye motif increases lipophilicity of the probe and thus, facilitates ligand internalization. Nevertheless, the mechanism of cellular internalization of Cy5.5-GX1 requires further investigation. Identification of the specific binding receptor for GX1 peptide is underway to unveil the mechanism. The approaches used in identifying the specific target include in vitro receptor-based screening and in silico bioinformatic analysis. Ongoing work also contains CD31 staining of U87MG tumor sections to further investigate the tumor vasculature status.

Cy5.5-GX1 was evaluated in the subcutaneous U87MG glioblastoma xenograft mouse model to examine its tumor-targeting efficacy. In vivo optical imaging studies showed U87MG tumors were clearly visible with high contrast to contralateral background at all measured time points after injection. The Cy5.5-GX1 probe exhibited a fast U87MG tumor targeting (as early as 0.5 h p.i.) and excellent tumor-to-background contrast at 4 h p.i. Both the tumor and normal tissue demonstrated rapid probe uptake. However, the probe washout in tumor is much slower than normal tissue, leading to excellent tumor-to-normal tissue contrast at later time points (after 4 h p.i.). For the non-blocked group, Cy5.5-GX1 exhibited the high contrast tumor-to-tissue ratios for imaging and detection. Scans of dissected

tissues and organs were consistent with in vivo imaging findings. Aside from the U87MG tumor, liver uptake of Cy5.5-GX1 remained higher than the amounts measured in other major organs, including kidneys, suggesting the hepatic pathway as the likely route of excretion. A blocking experiment was achieved by co-injection of Cy5.5-GX1 with unlabeled GX1 peptide (20 mg/kg). Significant reduced tumor uptake ($P < 0.05$) of Cy5.5-GX1 was observed for the blocked group at 4 h p.i., indicating Cy5.5-GX1 is a target-specific probe. Reduced uptake of Cy5.5-GX1 was observed in tissues during blocked experiments, mainly in the liver, kidneys, lung, spleen, and U87MG tumor, with the largest decrease in fluorescence in the tumor (Fig. 4c). Results suggest receptors of GX1 were sufficiently blocked in these organs using the 25 mg/kg amount of GX1.

Further methods to optimize the NIRF GX1 probes include careful selection of fluorescent labels and improvement of pharmacokinetic profile. We and others have showed that NIR fluorescent dye Cy5.5 can be used as a promising contrast agent for in vivo demarcation of tumors (Cheng et al. 2005; Chen et al. 2004; Weissleder et al. 1999; Ke et al. 2003; Petrovsky et al. 2003). However, the emission maximum of Cy5.5 at 694 nm is at the lower limit of NIRF region. Fluorescent dyes with more red-absorbing character may provide deeper tissue penetration and a better reflection of actual distribution of the probe in vivo. Quantum dots (QDs) would be a good alternative to the fluorescent dyes. As compared to organic fluorophores, QDs present unique optical and electronic properties, including size-tunable fluorescence emission from visible to NIR wavelength and high levels of brightness and photostability (Cheng et al. 2005; Gao and Nie 2005). Thus, the conjugation of GX1 peptide with QDs will be explored in further investigation. In addition, the optical imaging of Cy5.5-GX1 in U87MG tumor-bearing mice showed a considerable uptake in liver. Further modification is also needed to improve the pharmacokinetics of probe. For example, an appropriate linker may be incorporated into GX1 probe. However, the factor of length, flexibility, hydrophilicity, and charges (cationic, anionic, and neutral) of the linker needs to be carefully considered (Chen and Chen 2010). Finally, to obtain quantitative tumor-targeting and distribution patterns of the GX1-based probes, radionuclide imaging modalities such as PET or SPECT are warranted for future quantitative studies.

Conclusion

The Cy5.5 fluorophore was successfully conjugated with GX1 to image tumor vasculature. Cy5.5-GX1 provided highly sensitive and target-specific molecular imaging of tumors. It demonstrated excellent tumor-to-normal tissue ratio, fast tumor targeting ability, and rapid normal tissue clearance. Thus, Cy5.5-GX1 is a promising probe for imaging tumor vasculature in living subjects.

Acknowledgments This study was supported by Molecular Imaging Center, the USC Department of Radiology, and the Provost's Biomedical Imaging Science Initiative.

References

Achilefu S, Dorshow RB, Bugaj JE, Rajagopalan R (2000) Novel receptor-targeted fluorescent contrast agents for in vivo tumor imaging. Invest Radiol 35(8):479–485

Achilefu S, Jimenez HN, Dorshow RB, Bugaj JE, Webb EG, Wilhelm RR, Rajagopalan R, Johler J, Erion JL (2002) Synthesis, in vitro receptor binding, and in vivo evaluation of fluorescein and carbocyanine peptide-based optical contrast agents. J Med Chem 45(10):2003–2015

Beer AJ, Chen X (2010) Imaging of angiogenesis: from morphology to molecules and from bench to bedside. Eur J Nucl Med Mol Imaging 37(Suppl 1):S1–S3

Bergers G, Benjamin LE (2003) Tumorigenesis and the angiogenic switch. Nat Rev Cancer 3(6):401–410

Cai W, Chen X (2006) Anti-angiogenic cancer therapy based on integrin alphavbeta3 antagonism. Anticancer Agents Med Chem 6(5):407–428

Cai W, Gambhir SS, Chen X (2008) Chapter 7. Molecular imaging of tumor vasculature. Methods Enzymol 445:141–176

Castel S, Pagan R, Mitjans F, Piulats J, Goodman S, Jonczyk A, Huber F, Vilaro S, Reina M (2001) RGD peptides and monoclonal antibodies, antagonists of alpha(v)-integrin, enter the cells by independent endocytic pathways. Lab Invest 81(12):1615–1626

Charnley N, Donaldson S, Price P (2009) Imaging angiogenesis. Methods Mol Biol 467:25–51

Chen K, Chen X (2010) Design and development of molecular imaging probes. Curr Top Med Chem 10(12):1227–1236

Chen K, Chen X (2011) Positron emission tomography imaging of cancer biology: Current status and future prospects. Seminars in Oncology (in press)

Chen K, Conti PS (2010) Target-specific delivery of peptide-based probes for PET imaging. Adv Drug Deliv Rev 62(11): 1005–1022

Chen X, Conti PS, Moats RA (2004) In vivo near-infrared fluorescence imaging of integrin alphavbeta3 in brain tumor xenografts. Cancer Res 64(21):8009–8014

Chen B, Cao S, Zhang Y, Wang X, Liu J, Hui X, Wan Y, Du W, Wang L, Wu K, Fan D (2009) A novel peptide (GX1) homing to gastric cancer vasculature inhibits angiogenesis and cooperates with TNF alpha in anti-tumor therapy. BMC Cell Biol 10:63

Cheng Z, Wu Y, Xiong Z, Gambhir SS, Chen X (2005) Near-infrared fluorescent RGD peptides for optical imaging of integrin alphavbeta3 expression in living mice. Bioconjug Chem 16(6):1433–1441

Deutscher SL (2010) Phage display in molecular imaging and diagnosis of cancer. Chem Rev 110(5):3196–3211

Ellis LM, Liu W, Ahmad SA, Fan F, Jung YD, Shaheen RM, Reinmuth N (2001) Overview of angiogenesis: biologic implications for antiangiogenic therapy. Semin Oncol 28 (5 Suppl 16):94–104

Folkman J (1995) Angiogenesis in cancer, vascular, rheumatoid and other disease. Nat Med 1(1):27–31

Folkman J (2007) Angiogenesis: an organizing principle for drug discovery? Nat Rev Drug Discov 6(4):273–286

Gambhir SS (2002) Molecular imaging of cancer with positron emission tomography. Nat Rev Cancer 2(9):683–693

Gao X, Nie S (2005) Quantum dot-encoded beads. Methods Mol Biol 303:61–71

Hanahan D, Folkman J (1996) Patterns and emerging mechanisms of the angiogenic switch during tumorigenesis. Cell 86(3):353–364

Hui X, Han Y, Liang S, Liu Z, Liu J, Hong L, Zhao L, He L, Cao S, Chen B, Yan K, Jin B, Chai N, Wang J, Wu K, Fan D (2008) Specific targeting of the vasculature of gastric cancer by a new tumor-homing peptide CGNSNPKSC. J Control Release 131(2):86–93

Ke S, Wen X, Gurfinkel M, Charnsangavej C, Wallace S, Sevick-Muraca EM, Li C (2003) Near-infrared optical imaging of epidermal growth factor receptor in breast cancer xenografts. Cancer Res 63(22):7870–7875

Kerbel R, Folkman J (2002) Clinical translation of angiogenesis inhibitors. Nat Rev Cancer 2(10):727–739

Kobayashi H, Ogawa M, Alford R, Choyke PL, Urano Y (2010) New strategies for fluorescent probe design in medical diagnostic imaging. Chem Rev 110(5):2620–2640

Kuwano M, Fukushi J, Okamoto M, Nishie A, Goto H, Ishibashi T, Ono M (2001) Angiogenesis factors. Intern Med 40(7): 565–572

Mahmood U, Weissleder R (2003) Near-infrared optical imaging of proteases in cancer. Mol Cancer Ther 2(5):489–496

Massoud TF, Gambhir SS (2003) Molecular imaging in living subjects: seeing fundamental biological processes in a new light. Genes Dev 17(5):545–580

Moore A, Medarova Z, Potthast A, Dai G (2004) In vivo targeting of underglycosylated MUC-1 tumor antigen using a multimodal imaging probe. Cancer Res 64(5):1821–1827

Ocak I, Baluk P, Barrett T, McDonald DM, Choyke P (2007) The biologic basis of in vivo angiogenesis imaging. Front Biosci 12:3601–3616

Petrovsky A, Schellenberger E, Josephson L, Weissleder R, Bogdanov A Jr (2003) Near-infrared fluorescent imaging of tumor apoptosis. Cancer Res 63(8):1936–1942

Sancey L, Garanger E, Foillard S, Schoehn G, Hurbin A, Albiges-Rizo C, Boturyn D, Souchier C, Grichine A, Dumy P, Coll JL (2009) Clustering and internalization of integrin alphavbeta3 with a tetrameric RGD-synthetic peptide. Mol Ther 17(5):837–843

Tung CH (2004) Fluorescent peptide probes for in vivo diagnostic imaging. Biopolymers 76(5):391–403

Tung CH, Zeng Q, Shah K, Kim DE, Schellingerhout D, Weissleder R (2004) In vivo imaging of beta-galactosidase activity using far red fluorescent switch. Cancer Res 64(5):1579–1583

Ueberberg S, Schneider S (2010) Phage library-screening: a powerful approach for generation of targeting-agents specific for normal pancreatic islet-cells and islet-cell carcinoma in vivo. Regul Pept 160(1–3):1–8

Weissleder R (2006) Molecular imaging in cancer. Science 312(5777):1168–1171

Weissleder R, Mahmood U (2001) Molecular imaging. Radiology 219(2):316–333

Weissleder R, Tung CH, Mahmood U, Bogdanov A Jr (1999) In vivo imaging of tumors with protease-activated near-infrared fluorescent probes. Nat Biotechnol 17(4):375–378

Yancopoulos GD, Davis S, Gale NW, Rudge JS, Wiegand SJ, Holash J (2000) Vascular-specific growth factors and blood vessel formation. Nature 407(6801):242–248

Zhi M, Wu KC, Dong L, Hao ZM, Deng TZ, Hong L, Liang SH, Zhao PT, Qiao TD, Wang Y, Xu X, Fan DM (2004) Characterization of a specific phage-displayed peptide binding to vasculature of human gastric cancer. Cancer Biol Ther 3(12):1232–1235